PROCEEDINGS OF SPIE

NExtUP: the Normal-incidence Extreme Ultraviolet Photometer

Drake, Jeremy, Cheimets, Peter, Garraffo, Cecilia, Wargelin, Bradford, Youngblood, Allison, et al.

SPIE.

NExtUP: The Normal-incidence Extreme Ultraviolet Photometer

Jeremy J. Drake[*a], **Peter Cheimets**[a], **Cecilia Garraffo**[a], **Bradford Wargelin**[b], **Allison Youngblood**[b], **Vinay Kashyap**[a], **Paola Testa**[a], **David Caldwell**[a], **James Mason**[b], **Brian Fleming**[b], **Kevin France**[b], **Scott Wolk**[a], **Oswald Seigmund**[c], **Tommi Koskinen**[d], **Julián D. Alvarado-Gómez**[e], **Maria Mercedes Lopez-Morales**[a], **Guillaume Gronoff**[f], **Jay Bookbinder**[g], **Martin Barstow**[h], **David Windt**[i], **Randy Gladstone**[j], **Christopher Loghry**[k], **Rix Yarborough**[l]

[a]Center for Astrophysics | Harvard & Smithsonian, 60 Garden Street, Cambridge MA 02138
[b]Laboratory for Atmospheric and Space Physics, University of Colorado Boulder, Boulder CO 80303
[c]Space Sciences Laboratory, University of California, Berkeley CA 94720
[d]Lunar and Planetary Laboratory, University of Arizona, Tucson, AZ 85721
[e]Leibniz Institute for Astrophysics Potsdam, An der Sternwarte 16, 14482 Potsdam, Germany
[f]Science Systems and Application Inc., Nasa Langley Research Center, Hampton VA 23681, USA
[g]NASA Ames Research Center, Moffett Field, CA 94035
[h]School of Physics & Astronomy, University of Leicester, University Road, Leicester LE1 7RH, UK
[i]Reflective X-ray Optics, LLC
[j]Southwest Research Institute, San Antonio, TX 78228
[k]Moog, Inc., 21339 Nordhoff St., Chatsworth, CA 91311
[l]Arlington High School, 869 Massachusetts Ave, Arlington, MA 02476

Abstract. The Normal-incidence Extreme Ultraviolet Photometer (NExtUP) is a smallsat mission concept designed to measure the EUV radiation conditions of exoplanet host stars, and F-M type stars in general. EUV radiation is absorbed at high altitude in a planetary atmosphere, in the exosphere and upper thermosphere, where the gas can be readily heated to escape temperatures. EUV heating and ionization are the dominant atmospheric loss drivers during most of a planet's life. There are only a handful of accurately measured EUV stellar fluxes, all dating from Extreme Ultraviolet Explorer (EUVE) observations in the '90s. Consequently, current models of stellar EUV emission are uncertain by more than an order of magnitude and dominate uncertainties in planetary atmospheric loss models. NExtUP will use periodic and aperiodic multilayers on off-axis parabolic mirrors and a prime focus microchannel plate detector to image stars in 5 bandpasses between 150 and 900Å down to flux limits two orders of magnitude lower than reached by EUVE. NExtUP may also accomplish a compelling array of secondary science goals, including using line-of-sight absorption measurements to understand the structure of the local interstellar medium, and imaging EUV emission from energetic processes on solar system objects at unprecedented spatial resolution. NExtUP is well within smallsat weight limits, requires no special orbital conditions, and would be flown on a spacecraft supplied by MOOG Industries. It draws on decades of mission heritage expertise at SAO and LASP, including similar instruments successfully launched and operated to observe the Sun.

Keywords: Exoplanets, Stars, Flares, EUV, Space Missions, SmallSat, EUV optics, EUV detectors: MCPs.

*E-mail jdrake@cfa.harvard.edu

1 Introduction

1.1 Exoplanets and the Habitable Zone

Among the triumphs of astrophysics is the Kepler mission's finding, combined with ground observations, that planetary systems are common. With over 4,400 extrasolar planets confirmed[1], understanding which environments can support life is one of the next major challenges. Habitable planets are defined as those with an atmosphere able to sustain surface liquid water over billion year timescales. A major question for astrophysics in the next decades is what fraction of temperate, rocky planets around stars of different types can develop and retain a habitable atmosphere?

It has become clear that planetary surface temperature alone is not adequate to describe the habitable zone (HZ), and stellar optical-infrared radiation is insufficient to predict and interpret planetary biosignature gases [1, 2, 3, 4, 5] or evaluate rocky planets' potential to maintain habitable conditions [e.g., 6]. The stellar high-energy radiation environment, particularly EUV radiation, is the single largest forcing function for long-term habitability of exoplanet atmospheres.
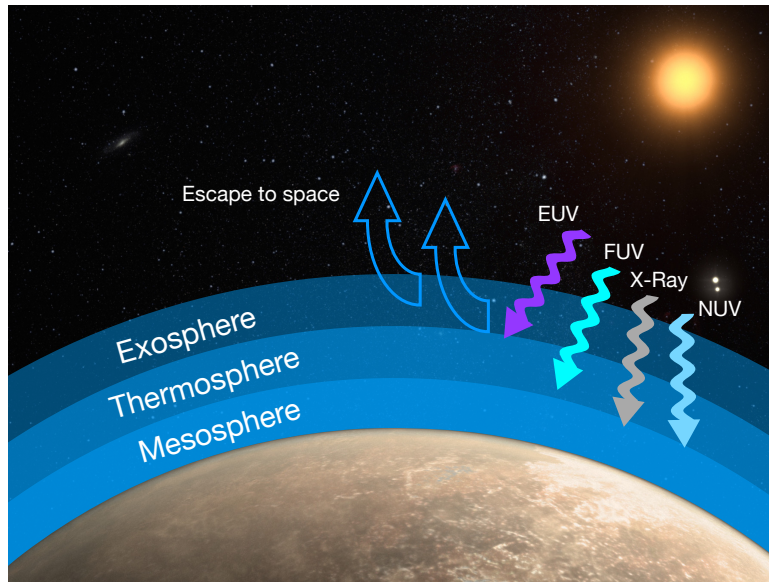
---

[1]https://exoplanetarchive.ipac.caltech.edu/

Fig 1 EUV radiation is the dominant driver of atmospheric loss. EUV radiation is absorbed in the exosphere and upper thermosphere where it can ionize and heat gas to escape temperatures and potentially drive hydrodynamic outflow. X-ray and UV radiation instead penetrate deeper and are generally less important for atmospheric loss.

1.2 Stellar EUV Radiation Drives Atmospheric Loss

The long-term habitability of an atmosphere is determined by the net loss of volatiles. Different parts of a star's spectral energy distribution (SED) drive heating and chemistry in different layers of a planet's atmosphere due to the wavelength dependence of atomic and molecular photoabsorption cross-sections (Figure 1). Optical and near-infrared photons heat the surface and troposphere while NUV (1800–3200 Å), FUV (912–1800 Å), and X-ray (5–100 Å) photons are absorbed in the middle and upper atmosphere where they photo-dissociate molecules. But it is EUV emission that is the key driver for atmospheric mass-loss.

EUV photons (100-911 Å) are absorbed very high in the atmosphere (the exosphere and upper thermosphere) due to the large photoabsorption cross-section. They ionize atoms and molecules, heating the gas and increasing the scale height of the atmosphere and potentially leading to the formation of a hydrodynamic outflow and rapid atmospheric escape [7]. In highly-irradiated planets, the outflow is rapid enough that heavier elements (e.g., O and C) can be dragged along with the lighter hydrogen, as observed on hot Jupiters [e.g., 8, 9, 10]. Free electrons produced by stellar EUV photons reach altitudes greater than ions, producing an ambipolar electric field that leads to additional non-thermal outflow [e.g., 6, 7, 11, 12]. EUV photons are more efficient per erg at heating the atmosphere than X-rays and more EUV than X-ray photons are emitted by stars to drive this heating. In the quiet Sun, the EUV/X-ray photon production ratio is 90 [13]. For optically inactive early M dwarfs the EUV/X-ray photon ratio is 40 [14], and even for an active later M dwarf the EUV/X-ray photon ratio is 16.

The stability of Earth-like atmospheres, therefore, depends on the EUV irradiance [e.g., 15]. The University of Colorado (CU)-led Mars Atmosphere and Volatile Evolution (MAVEN) mission has confirmed the importance of EUV-driven mass loss on Mars [16]. Higher EUV flux from the young Sun [17] could have led to 10 times greater oxygen loss rates and 90 times greater carbon loss rates by increasing the suprathermal or "hot" population of these atoms [18].

Rocky planets around M-dwarf stars ($3850 \geq T_{eff} \geq 2300$ K) will likely be the only potentially habitable planets whose atmospheres will be searched for signs of life with the upcoming JWST and extremely large telescopes [ELTS; 19, 20, 21] prior to a large UVOIR mission in the 2030s or 2040s[2]. M dwarf exoplanets are particularly prone to EUV-driven atmospheric escape: scaling relations indicate EUV irradiance factors of ~10 times the average solar value owing to the close-in HZ [22, 23]. Additionally, the EUV luminosity of M dwarfs is enhanced by another $10\times$-$50\times$ during their

---

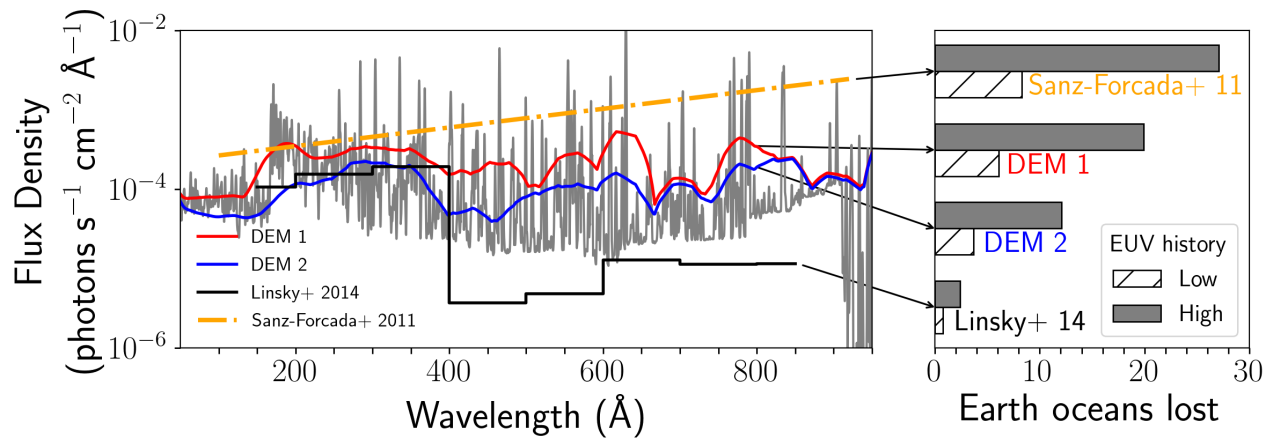[2]LUVOIR Team Final Report; https://asd.gsfc.nasa.gov/luvoir/reports/

Fig 2 Left: Different reconstructions of the EUV spectrum of the M dwarf Proxima Cen show $3\times$-$100\times$ flux discrepancies: differential emission measure models in red, blue, and gray [25]; scaling relations based on only FUV in black [26] and on X-rays in orange [27]. Right: Corresponding hydrogen mass lost from an Earth-like planet (in units of Earth oceans) from 10 Myr to 4.8 Gyr for high (shaded gray) and low (hatched) EUV histories of typical M dwarfs [28]. NExtUP EUV fluxes would eliminate this huge uncertainty in atmospheric loss rate.

long pre-main-sequence and spin-down evolution, the latter lasting up to several Gyrs longer than Sun-like stars, into or beyond the era when life emerged on Earth.

The discovery of rocky planets in the HZs of nearby stars, e.g., Proxima Cen b and the TRAPPIST-1 planets, has motivated new atmospheric mass loss calculations that highlight the need for improved EUV irradiance data to assess their long-term habitability. Studies of EUV-driven ion loss from Earth-like planets orbiting M dwarfs found mass loss rates several orders of magnitude higher than that of present-day Earth for EUV fluxes $10\times$-$20\times$ the present day EUV solar irradiance [23, 24]. Elevated EUV fluxes, augmented by persistent flares or the long pre-main-sequence and spin-down phases of M dwarfs, could render some Earth-like planets around M dwarfs barren in the absence of internal or external resupply of volatiles.

Rapid atmospheric loss can lead to desiccation and the build-up of abiotic O_2 atmospheres that complicate biomarker searches [29, 30, 31]. Figure 2 shows the results of atmospheric escape calculations for Proxima Cen b under different EUV radiation strengths and histories. Model calculations yield a $30\times$ spread in the atmospheric mass loss from the planet over time, driven mostly by a lack of firm constraints on the current EUV flux and its evolution earlier in the star's history.

1.3 The need for NExtUP

EUV flux measurements of exoplanet host stars are currently very scarce. The only previous dedicated EUV astronomy mission, the Extreme Ultraviolet Explorer [EUVE; 32, 33], obtained spectra of 15 cool main sequence stars, including 5 early M-type dwarfs. These observations were heavily biased toward the most active stars. The very modest effective area of the EUVE spectrometers precluded useful spectroscopic observations of stars with more solar-like activity, except for the α Cen system and the F4 subgiant Procyon [e.g. 34, 35]. No observed EUV spectra exist of optically inactive M dwarfs [i.e., Ca II H & K equivalent widths < 1.0 Å, e.g., 36, 37], or late M-dwarfs such as TRAPPIST-1 that will be optimal for biosignature searches with JWST, 30m telescopes, and the *Origins* Space Telescope. The lack of direct EUV data hampers our ability to understand how habitable atmospheres evolve with time, and to design truly definitive biosignature searches. Consequent orders of magnitude uncertainties in ion escape rates can fundamentally shift our predictions for which exoplanets are the best candidates for long-lived habitable atmospheres.

Stellar atmosphere codes that can predict the EUV emission for individual stars by self-consistently modeling a chromosphere, transition region, and corona are in their infancy [e.g., 14, 38]. In lieu of predictive physical models, EUV scaling relations with FUV and/or X-ray emission are commonly used to approximate the EUV environment in which planets orbit [22, 26, 27, 39]. These approaches have significant shortcomings: while X-rays are generated in the stellar corona ($T > 10^6$ K) and FUV photons are generated in the chromosphere and transition region ($T < 10^5$ K), none of the scaling relations are based on the $10^5 - 10^6$ K range of atmospheric temperature where most of the 170–900 Å emission is produced, and consequently there are order of magnitude difference in EUV scaling prescriptions leading to $> 10\times$ uncertainties in atmospheric mass loss rates (Figure 2).
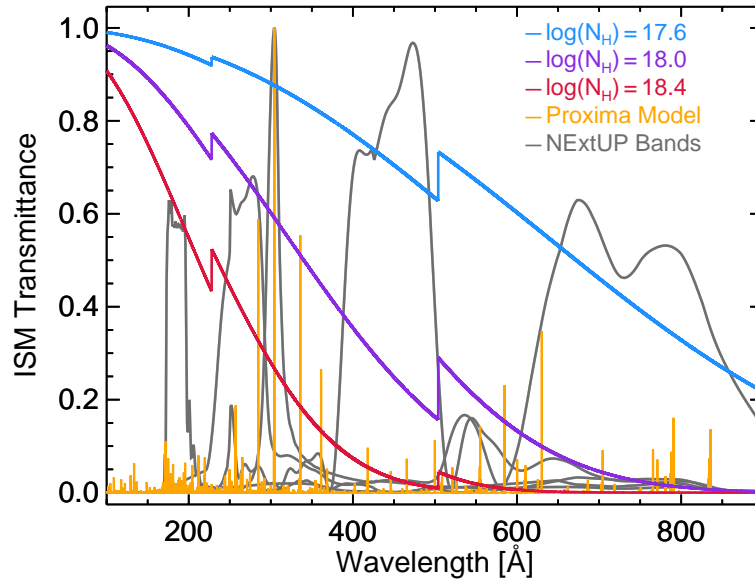
Fig 3 Transmittance of the local interstellar medium for H I column densities typical of stars within 30pc ($10^{17.6} - 10^{18.4}$ cm^{-2} [40, 41]) superimposed over an EUV spectral model for the M5.5 dwarf Proxima Centuri and the provisional NExtUP bandpasses. The ISM is more than 20% transparent to EUV photons over most of the NExtUP wavelength range for most stars within 30 pc.

2 Observability of Stars in the Extreme Ultraviolet

The National Academy of Sciences report on Exoplanet Science Strategy highlights the central importance of the EUV waveband for understanding atmospheric evolution. However, the report also states "EUV fluxes are not accessible due to the attenuation of the interstellar medium". This is indeed generally true for large distances (> 100 pc for example). But nearby stars can be readily observed in the EUV, as was demonstrated by the EUVE all-sky survey [33].

Figure 3 illustrates the ISM transmittance for various neutral hydrogen (H I) column densities. The nearest stars——the α Centauri system—have H I absorbing columns of $10^{17.6}$ cm^{-2} [40]. The solar system resides in the local ISM cloud complex, which itself appears to lie in a lower density "local bubble" [42, 43, 44, 45]. Despite the physical complexity of the local ISM, integrated H I column density N_H (the most relevant parameter for EUV transmission) rarely exceeds $10^{18.4}$ cm^{-2} within 30 pc of the Sun [40]. Stars within 30 pc encompass almost all HZ planets that are candidates for spectroscopic characterization and biomarker detection (LUVOIR Team Final Report). NExtUP would have the sensitivity to detect EUV emission with good signal-to-noise for nearly all F, G, K and active M stars out to 30 pc, and for low mass M dwarfs and inactive stars out to ~ 12 pc.

In short, the interstellar medium is not the limiting factor in our ability to study EUV emission from the most important exoplanet hosts.

3 The NExtUP Observatory

NExtUP utilizes 3 decades of imaging expertise developed at Smithsonian Astrophysical Observatory (SAO) and the Laboratory for Atmospheric and Space Physics (LASP) for observing the Sun in the UV and EUV to observe similar activity of nearby stars. The observatory has five prime focus channels (presently named A, B, 304, C and SiC) housed inside an EELV Secondary Payload Adapter (ESPA) Grande spacecraft, dedicated to the study of stellar EUV emission. An artists impression of NExtUP in orbit is presented in Figure 4.

3.1 Mirrors

Each of the five NExtUP channel consists of a 25 cm diameter off-axis parabolic mirror and an out-of-band UV/optical blocking filter; the light from all channels is focused on a common microchannel plate detector. The focal length of the system is 127 cm, and is maximised by the spacecraft and instrument design that provides the longest practical optical
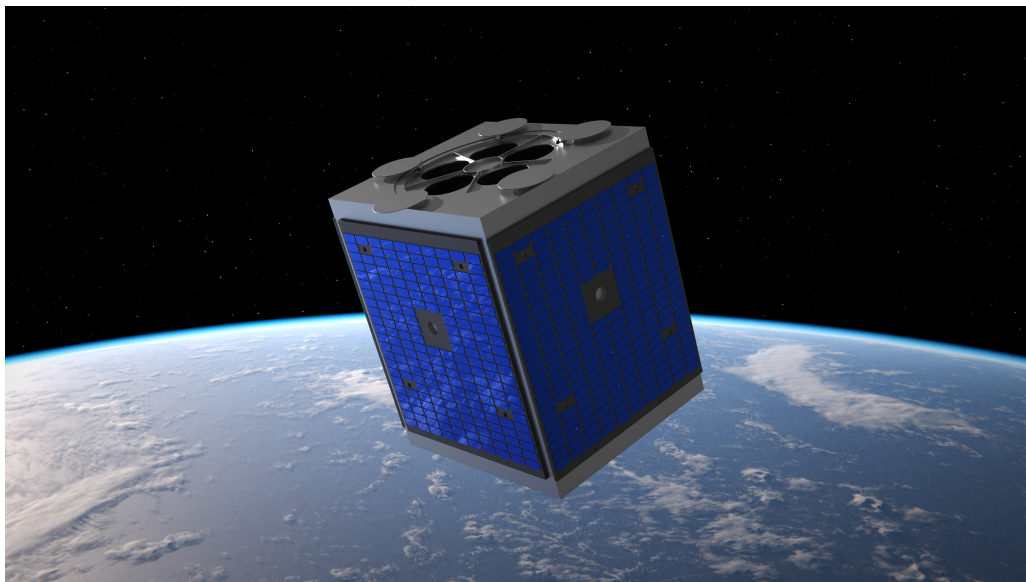
Fig 4 An artists impression of the NExtUP Observatory in orbit. Solar panels are affixed to four sides of the Moog Inc. spacecraft, enabling flexible orientation with respect to the Sun. The spacecraft is attached to the ESPA ring at the opposite end to the telescope entrance apertures for launch.
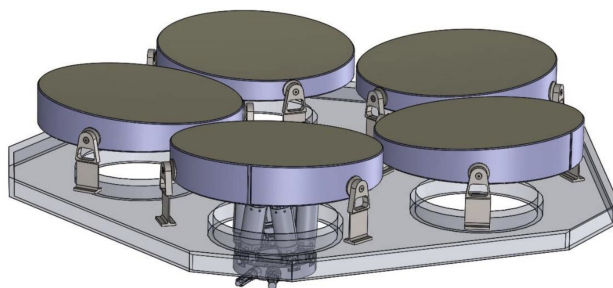

Fig 5 The NExtUP mirror system comprising five 25 cm diameter off-axis parabolas aligned to a common prime focus microchannel plate detector. The mirror mount flexures (three per mirror) and hexapod alignment device (front centre) can also be seen.

bench length within the tolerances of the ESPA ring system. By operating at prime focus, we maximize effective area by minimizing reflection losses. The optical elements are described below in the order in which they are encountered in photon flight.

The spacecraft back plate has five mirror mounts. Each mirror is bonded to three flexures, utilizing a mirror design successfully employed in multiple missions. The flexures maintain mirror position and figure while providing isolation from external forces. The mirrors are positioned and aligned using a GSE Hexapod PM Alignment system to focus onto a specific place on the detector (Figure 5). The separate mirrors are mounted slightly offset (~ 10 mm) from a point at which they would share a common axis.

The mirrors will be Zerodur$^{\mathrm{TM}}$ with a near zero coefficient of thermal expansion (CTE), while the flexure bonding pads are Invar$^{\mathrm{TM}}$ connected to the Titanium flexure. Hysol 9313 adhesive will be used to bond the mirrors to the flexures—a technique first developed for the *Chandra* mission and used in several other missions since. The system results in a strong, temperature insensitive support with minimal outgassing.

3.2 Multilayer Coatings

The telescope design uses multilayer coatings that provide high EUV reflectance at normal incidence. A multilayer coating exploits the principle of optical interference to achieve high reflectance, and comprises a stack of layers of two
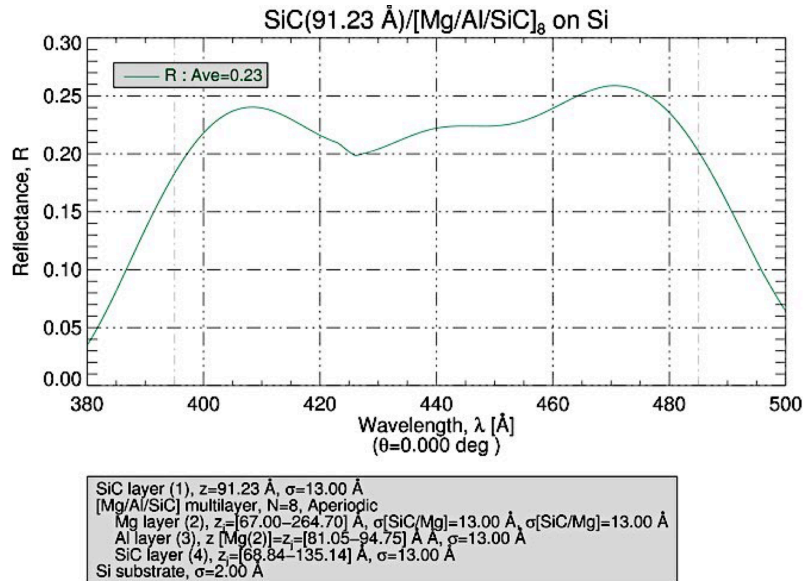
SiC(91.23 Å)/[Mg/Al/SiC]₈ on Si

SiC layer (1), z=91.23 Å, σ=13.00 Å
[Mg/Al/SiC] multilayer, N=8, Aperiodic
  Mg layer (2), z_2=[67.00–264.70] Å, σ[SiC/Mg]=13.00 Å, σ[SiC/Mg]=13.00 Å
  Al layer (3), z [Mg(2)]=z_3=[81.05–94.75] Å, σ=13.00 Å
  SiC layer (4), z_4=[68.84–135.14] Å, σ=13.00 Å
Si substrate, σ=2.00 Å

Fig 6 Multilayer reflectivity as a function of wavelength at normal incidence for the NExtUP Channel C. The aperiodic design allows for a fairly flat reflectivity curve over a wide ~ 80 Å range.

or more materials, with individual layer thicknesses designed to optimize the reflectance over a desired spectral band-pass. Multilayers can be period or aperiodic. A periodic multilayer is a film stack containing a number of repeating, identical groups of layers, typically bi-layers or tri-layers (that is, using 2 or 3 different materials, respectively). Periodic multilayers provide high reflectance over a narrow spectral band-pass, and are designed parametrically.

An aperiodic multilayer is a film stack containing non-repeating layer groups, is designed numerically, and is typically used to achieve high reflectance over a broad spectral band-pass, generally at the expense of peak reflectivity. Periodic multilayers for solar physics have a flight heritage spanning several decades. The more recently developed aperiodic coating technology is only now just emerging for use in instrumentation for solar physics and other applications, and represents one of the enabling innovations for NExtUP.

Each mirror is coated with a tuned multilayer to reflect only a specific EUV band, and the coating and the focal plane filter control the operative wavelength of the channel. Similar approaches have been employed in solar missions, but NExtUP is innovative in utilizing them for an astrophysical application.

The baseline multilayers for NExtUP are listed in Table 1. Channel A employs an aperiodic Al/Zr coating that was recently developed and experimentally demonstrated. Periodic Al/Zr multilayers have been used for the Hi-C solar mission [46]. Channels "304", C, and "SiC" use multilayers made from Al, Mg, and SiC layers [47]. The "304" channel uses a periodic design to observe the Lyman α transition of He II 304 Å, which is the single brightest EUV line in typical stellar EUV spectra. The C and "SiC" channels use aperiodic designs.

Aperiodic Al-Mg/SiC coatings were recently used for the ESIS solar mission[3]. Channel B uses an aperiodic coating made from Zr, Co, and Mg layers; while this particular aperiodic coating design has not yet been tested, periodic Zr/Co/Mg multilayers have already been experimentally demonstrated and show excellent performance [48]. The exact aperiodic multilayer designs for NExtUP will depend on optical performance of test samples and remain somewhat flexible.

An example NExtUP multilayer coating design for Channel C is illustrated in Figure 6. Multilayers have excellent off-band rejection, although typically can have some throughput in higher harmonics and longward of the target wavelength. Of special concern is throughput in the vicinity of the geocoronal He I 584 Å line that is a potentially significant source of background. This wavelength is designed to be strongly suppressed by the NExtUP UV/optical blocking filters and by the multilayer design itself.

---

[3]https://www.montana.edu/news/19196/new-msu-instrument-collects-sun-data-aboard-nasa-rocket

Channel	Bandpass (FWHM, Å)	Coating	No. Layers Periodic/ Aperiodic	Peak Reflectivity	Required Eff. Area (cm²)	Predicted Eff. Area (cm²)	Luxel Filter
A	170-203	Al/Zr	60/A	0.24	**17.5**	21.0	Al 600 Å + C 150 Å
B	226-302	Zr/Co/Mg	10/A	0.29	**19.0**	23.0	Al 600 Å + C 150 Å
304	288-323	Al-Mg/SiC	1-40/P	0.34	**27.5**	33.0	Al 600 Å + Si 400 Å
C	381-409	SiC-Mg/Al/SiC	1-8/A	0.26	**27.0**	32.0	Al 600 Å + Si 400 Å
"SiC"	600-921	SiC-Al-Mg-SiC/Mg	1-1-1-10/A	0.50	**17.5**	21.0	Sn 700 Å

Table 1 The NExtUP bandpasses specification. Listed are the bandpass wavelengths (defined as the wavelength region were the effective area is > 10% of the peak area), multilayer coating specifications and peak reflectivity, required and predicted effective areas, and UV/optical blocking filter specifications.
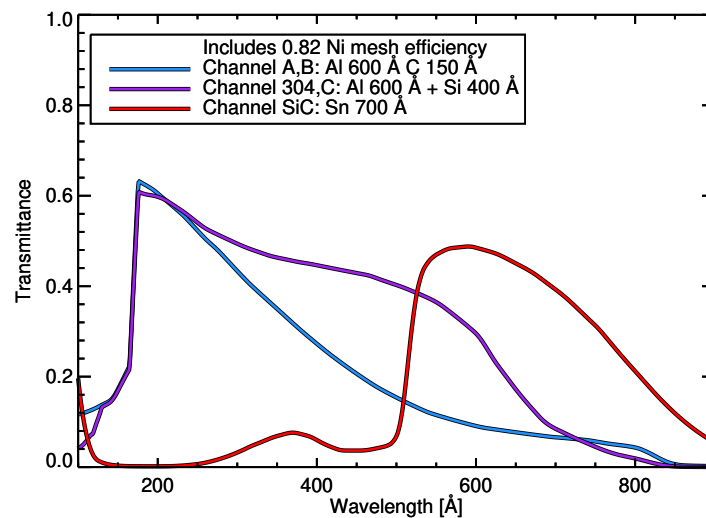

Fig 7 The NExtUP filter transmittance curves for the three different filter designs. Channels A and B share the same design, as do channels 304 and C.

3.3 UV/Optical Blocking Filters

The focal plane filters are metal films tuned to the different channels, supported on 82% open nickel mesh. The filters exploit material transmittance properties to limit the amount of off-band light in each channel. Specifications are listed in Table 1. Channels A and B use Al filters with carbon added to attenuate long-ward EUV and 584 Å background. Channels 304 and C use a similar design except with an Si overlayer. Channel "SiC" uses an Sn filter. The filters are near the focal plane and small (6.3mm diameter), and consequently robust to launch stresses; they also help to baffle stray light.

The filter transmittance curves for the three different filter designs are illustrated in Figure 7.

3.4 Microchannel Plate Detector

The NExtUP sensor is a photon counting, imaging microchannel plate (MCP) detector with atomic layer deposited (ALD) MCPs [49, 50] and a cross delay line (XDL) readout [49, 50, 51, 52, 53, 54, 55, 56], see Figure 8. The format is 38 mm diameter round with a potassium bromide EUV sensitive photocathode, built by the University of California, Berkeley (UCB)-Space Sciences Laboratory (SSL). MCP detectors have a long history in NASA space missions, including the HST-COS, EUVE, GALEX, SOHO, GOLD, EMM-EMUS and ICON [32, 51, 52, 53, 54, 55, 56, 57, 58, 59, 60] systems built by UCB. The NExtUP detector is circular in format and a copy of the one flown on GOLD and the EMM-EMUS detectors.
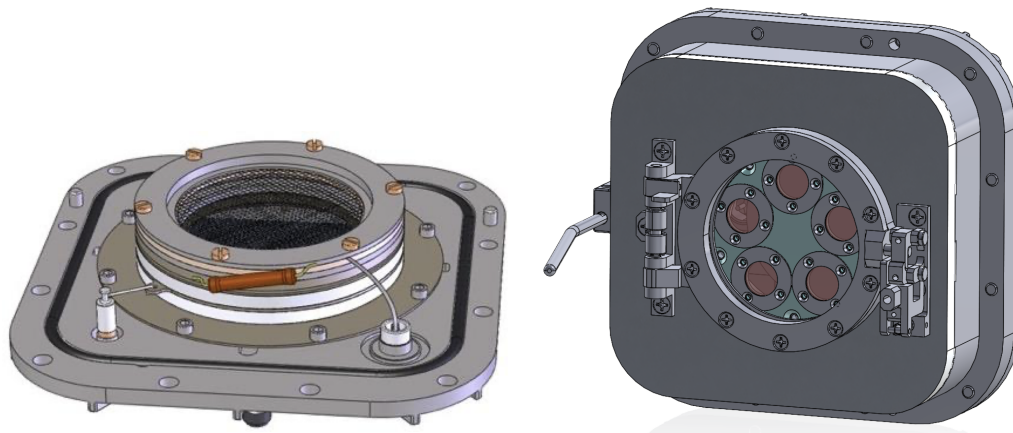
Fig 8 Detail of the NExtUP MCP detector (left) and its housing (right). The detector is circular with a diameter of 38 mm. The five focal plane UV/optical blocking filters are mounted in machined recesses in the detector housing, and are situated behind the saphire glass detector door.
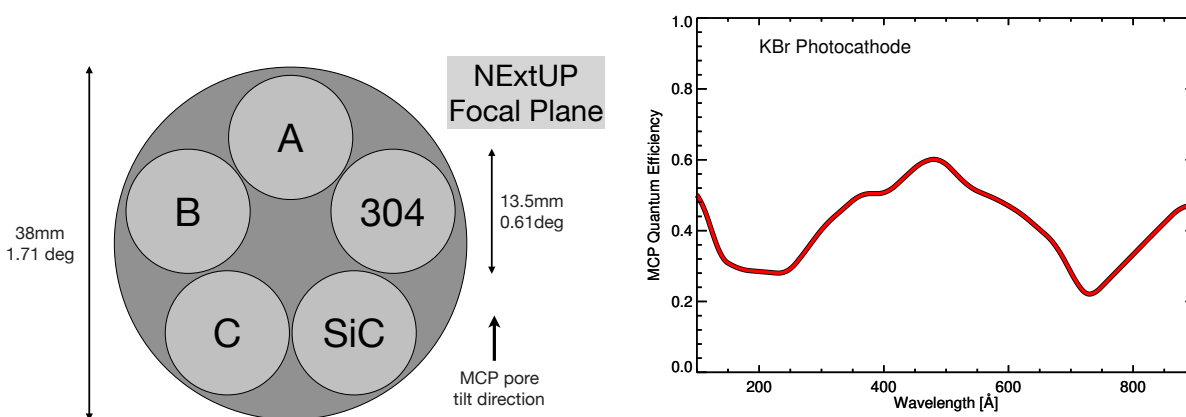

Fig 9 Left (a): The layout of the different NExtUP channels on the focal plane. The arrangement of the channels maximises the quantum efficiency for the converging light cone of the different channels, with the shorter wavelength channels requiring a less steep angle of incidence relative to the MCP pores that the longer wavelength channels. Right (b): The average MCP quantum efficiency as a function of wavelength for the slated KBr photocathode close to normal incidence.

Photons are detected by the photocathode on the MCP, and amplified by a factor 10^7 by the MCPs and high voltage potential across them. The photocathode is generally coated to enhance photoelectron production; NExtUP will employ KBr coatings which offer good quantum efficiency through the EUV band. Each photon event position is deduced from the difference in signal arrival times at the ends of X and Y delay lines.

UCB MCP detectors in LEO orbit show that the background is dominated by indirect radiation events converted by the satellite and detected by the MCPs and is proportional to satellite mass. Since ALD MCP background is < 0.1 events cm^{-2} s^{-1} [61] the low mass of NExtUP produces low background estimated to be 0.3 count cm^{-2} s^{-1}.

The detector provides approximately 1k x 1k resolution elements using electronics identical to those in recent planetary programs [56, 62, 63, 64, 65, 66]. Global counting rates of > 1 MHz, and local rates of > 1 kHz/resel have been demonstrated [63].

The NExtUP detector resides inside a vacuum housing with a manually reclosable door to isolate it from contamination (Figure 8). The door is actuated by a TiNi puller, based on heritage from several successful systems [62, 63, 64, 67, 68]. It allows dry N$_2$ backfill [69], which maintains performance over long durations during handing [62, 70, 71]. There is a window in the door over the active area to allow testing and operation during the I&T flow. Optical sensors are used to indicate the door open/closed positions.

The detector is implicitly divided into 5 regions (see Figure 9a), each dedicated to the light from a channel. The five channels are arranged in a circular pattern that maximizes their quantum efficiencies (QE) by matching the incidence
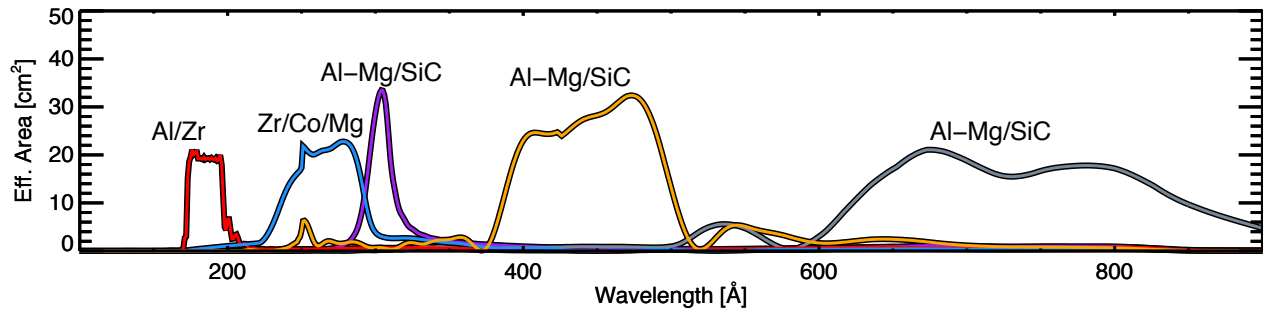
Fig 10 The NExtUP effective area curves as a function of wavelength for the five different channels, labelled with their respective multilayer coatings. From left to right the channels are A, B, 304, C and SiC.

angle of the incoming light cone with the peak of the QE vs incidence angle for the average photon energy of each channel (Figure 9a). The average detector quantum efficiency as a function of wavelength for the KBr photocathode NExtUP would employ is shown in Figure 9b.

Baffles near the detector and clear of the detector door serve to isolate the light from a given channel and block light from other channels from entering. The detector is supported by a titanium pentagonal tube. There is a plate at the instrument center of mass to mount to the spacecraft. The outer plate defines the entrance apertures, and supports the detector.

3.5 Detector Electronics

The NExtUP detector high voltage power supply (HVPS) and readout system is based on technology development carried out for the Colorado University cubesat SPRITE (launch date in 2022), which features a similar MCP and identical detector electronics [72, 73]. The design of both systems is based on several sub-orbital MCP detectors developed at CU [37, 74]. The NExtUP HVPS uses an Advanced Energy UltraVolt 6AA12-N4 module in a miniaturized radiation-tolerant printed circuit board (PCB) package. The output is interfaced to the detector with two Reynolds high voltage (HV) coaxial connections and is reconfigurable on-orbit with a 16-bit digital to analog converter DAC control signal to any voltage output between 0 to −6000 V with 92 mV resolution. A switch driven by a shift register Integrated circuit (IC) transitions the HV output between an active and a standby (approximately −3600 V) voltage to deactivate the detector in the South Atlantic Anomaly (SAA) or during downlink or battery charging. The input current is throttled to protect the MCP at coronal pressures (0.01 − 10 torr).

The readout system converts the low-voltage differential signaling (LVDS) signals from the detector electronics into two 16-bit data words for downlink. Each 16-bit word contains a 1-bit identifier (0 for X, 1 for Y), 11 bits for X or Y position of the photon event, 3 bits of the 6-bit total pulse height, and 1-bit of the total 2-bit counter for arrival time. The counter is a relative measure of the arrival time of each photon. The timing resolution can be as short as milliseconds.

The MCP registers the photon arrival and detector position; its arrival time is logged by the read out electronics. Photon arrival information is downlinked to Earth with instrument aspect information. Spacecraft pointing data, instrument calibration, and ancilliary data are used to adjust the arrival position, removing thermal and pointing jitter effects, as demonstrated on *Chandra*, HST and GALEX.

3.6 Effective Areas

The effective areas of the different NExtUP channels are the product of the geometrical areas of the mirrors, the mirror reflectivities, the filter transmittance and the MCP QE. The effective area curves are illustrated in Figure 10.

The NextUP bands are designed to capture important groups of bright spectral lines formed at different temperatures through the EUV range. The 304 channel is specifically designed to capture the bright He II 304 Å line. Figure 11 illustrates the emission intensity of an optically-thin collision-dominated plasma as a function of wavelength and plasma temperature and is superimposed with the NExtUP bandpasses. The He I 584 Å line is specifically avoided as geocoronal 584 Å emission is a potentially problematic source of background.
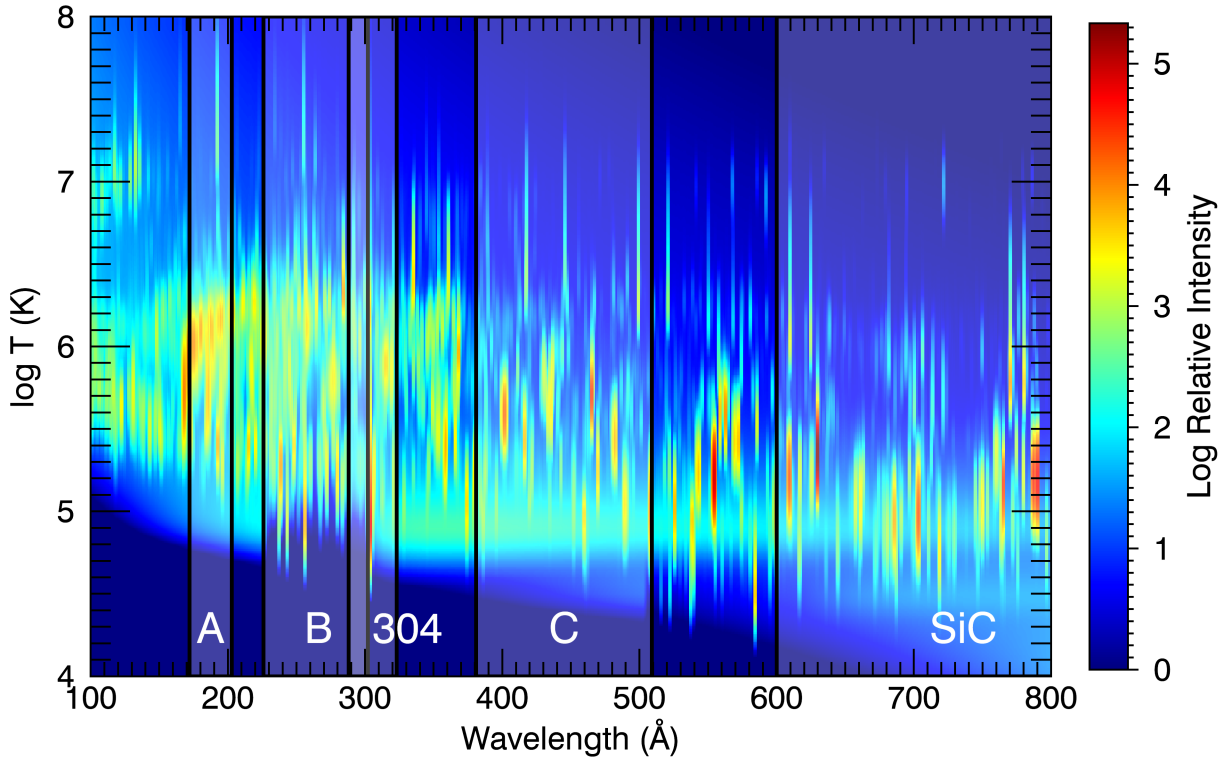
Fig 11 Emission intensity of an optically-thin collision-dominated plasma as a function of wavelength and plasma temperature, overlayed with the nominal NExtUP bands.

3.7 Imaging Resolution

NExtUP counts photons. When a photon arrives its detected position and arrival time are captured. The image is created once the observation is complete. This is done by taking the photon arrival information, the known pointing line of sight at arrival time, and estimates of the telescopes' internal distortion to adjust the photon's position on the sky. A cross check exists in NExtUP because of the shared structure between channels. We will use common mode effects in multiple channels to verify and improve the aspect solution.

There are 2 main contributors to the final imaging resolution: the resolution of the MCP detector (5.7 arcsec FWHM), and the pointing knowledge repeatability of the star tracker (5.7 arcsec root mean square (RMS), coincidentally) updated at 4Hz. Photons arrive at random times between star tracker updates. The observatory pointing is interpolated based on the proximate star tracker updates. The accuracy of this approach is set by the repeatability of the star tracker output, and spacecraft jitter. We predict a pointing uncertainty of 5.1 arcsec FWHM by combining the output from 2 star trackers, and averaging them over a second, and combining the result, in quadrature, with the predicted jitter rate of 1.8 arcsec FWHM. The combination of these effects, and a few smaller contributors, are shown in Table 2.3.5-1. The predicted resolution is 7.7 arcsec FWHM.

3.8 Instrument Control

The operation of the NExtUP instrument is simple: once the MCP is powered up, it begins to register incoming photons. It will continue to do that as long as there is power and the HV is supplied to the MCP. The stellar source is selected by pointing the observatory. An instrument controller will store the MCP counts data as they occur for later downlinking. The only active electronics in the instrument are those associated with the MCP itself. The telescope aperture doors and the instrument door are the only moving parts on NExtUP; these are operated only once at deployment. There are no moving parts in NExtUP following deployment and during science operations.
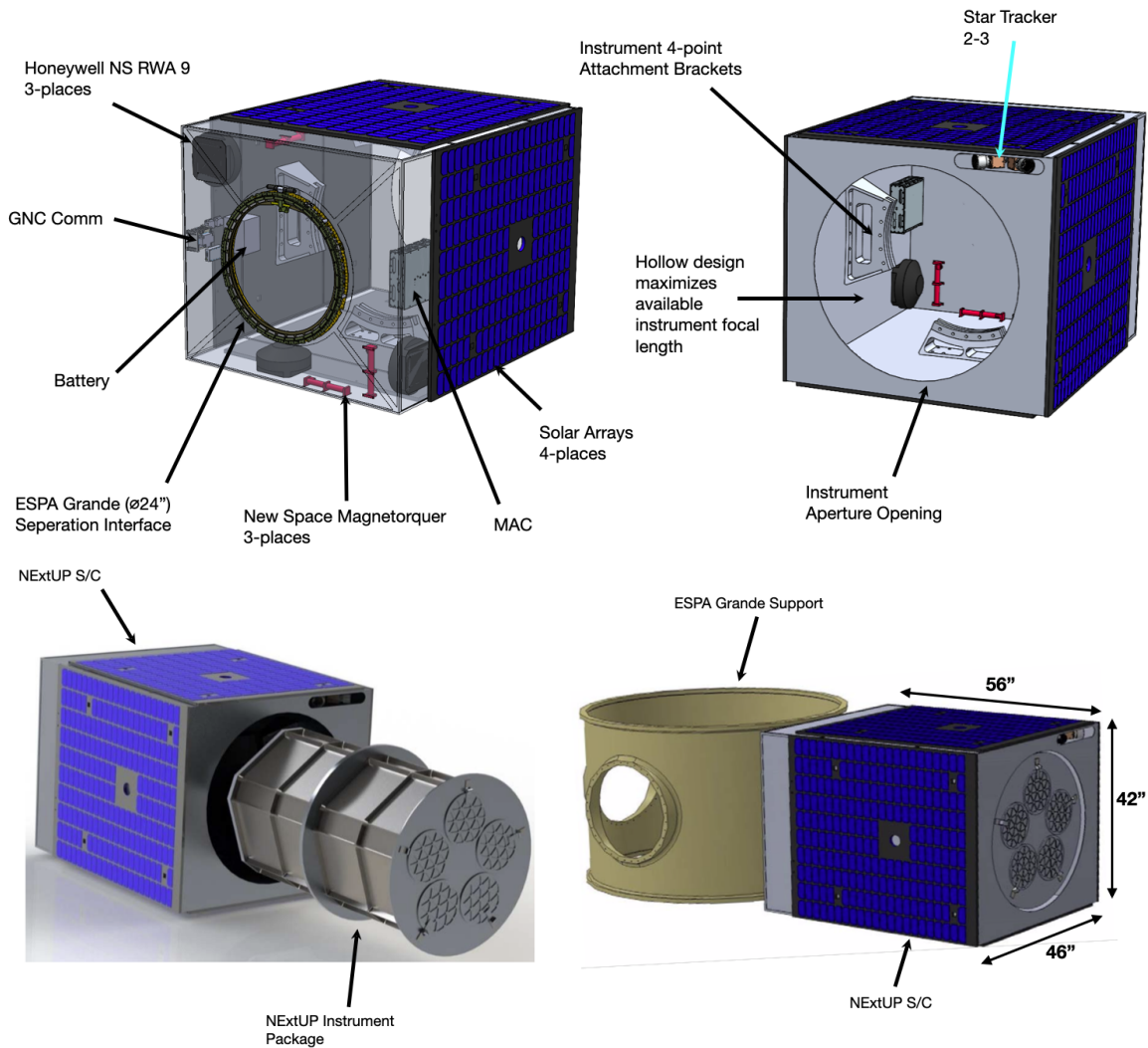
Fig 12 Details of the NExtUP Moog spacecraft. The hollow design maximises the available instrument focal length. The instrument package consists of a cylindrical structure fixed to spacecraft with an interface ring close to the center of gravity. The spacecraft is designed to attach to an ESPA Grande ring.

4 Spacecraft

The Moog Inc. spacecraft conforms to the volume allowed as part of the ESPA Grande launch option and contains all necessary avionics, power, guidance, navigation and control (GNC), and bus communications hardware. The NExtUP instrument is fully enclosed by the spacecraft and does not protrude into the ESPA interface ring. (Figure 12). The platform is 3-axis stabilized using reaction wheels and torque rods. The system does not have propulsion, reducing complexity and difficulties with manifesting.

The spacecraft Bus is an aluminum box/panel structure that provides radiation shielding, electromagnetic interference/electromagnetic compatibility (EMI/EMC) mitigation, and acts as a thermal radiator. The NExtUP instrument is mounted in the Bus central cylinder with the optical bench attached to integral points on the structural frame (Figure 12). The box/panel construction allows for easy integration and test.

The spacecraft has a 24" Motorized Light Band (MLB) attached for mounting to the 5-meter fairing of the ESPA Grande port interface ring. The combined mass of the spacecraft and NExtUP instrument (including 15% margin on each) is 304 kg which is over 35% below the 465 kg capacity of the ESPA Grande port. Concept design shows the CG to be on the central axis of the interface ring and less than 0.5m (20 inches) from the port mounting surface.
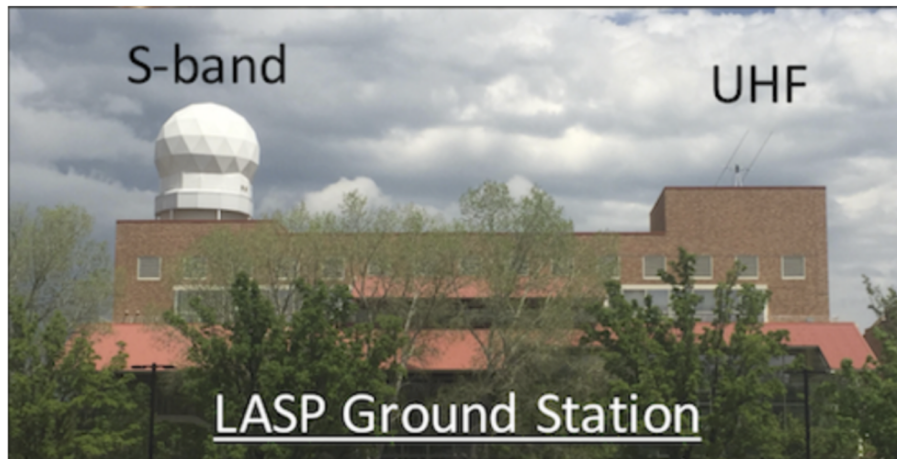
Fig 13 The CU LASP ground station that will handle NExtUP mission operations. LASP has more than 5 decades of experience flying NASA missions and instruments big and small.

The bus GNC system employs multiple modes of operation to meet the requirements of the mission. It uses Commercial Off The Shelf (COTS) components with flight heritage. The GNC actuators consist of three 8 N-m-s reaction wheels and three 26 A-m2 magnetic torque rods. During operations the reaction wheels provide precision payload pointing and the torque rods offload momentum as required.

The bus will utilize an Innoflight SCR-100 S-Band transceiver to meet the needs of the payload and the vehicle. The S-band link will utilize two antennas to provide coverage in a large range of spacecraft attitudes (tumbling, sun-pointing and nadir pointing).

5 Mission Operations and Data Products

The NExtUP Mission Operations Center would be based at CU LASP (Figure 13), leveraging LASP's experience on missions including: Magnetospheric Multiscale Mission (MMS), Global-scale Observations of the Limb and Disk (GOLD), and Compact Spectral Irradiance Monitor Flight Demonstration (CSIM) and Kepler mission, with IXPE and IMAP coming soon.

NExtUP communications would be via three passes per day in S-band, with an estimated conservative data rate of 110MB/day. The photon event data is expected to be dominated by the out-of-band He I 584 Å airglow.

The LASP operations team will provide command, control and planning support using the same OASIS software used for other missions. This includes monitoring the spacecraft operations, scheduling with the ground station network and troubleshooting and resolving anomalies.

Data will be formatted in compliance with International Virtual Observatory Alliance (IVOA) requirements. These include time tagged event lists and aspect pointing information, together with higher-level data products such as aspect-corrected images. Data products will be available to the community immediately after verification and validation through the Center for Astrophysics.

6 Target Selection and Observing Strategy

NExtUP attacks its science objective through a combination of four observing strategies. These are: Short Integration NExtUP (SHINE) observations; Long NExtUP Stare (LONESTAR) observations; NExtUP Ultracool dwarf Survey (NExUS), and NExtUP Targets of Opportunity (NExtOP).

SHINE will perform efficient, generally short ($\sim 1 - 10$ ks) integrations of a large sample of ~ 200 stars to measure their EUV fluxes to a $S/N \geq 10$. A subset of 25% of SHINE targets would be observed 5 times, separated by days to months, to measure EUV long term variability.

LONESTAR will undertake long 100ks observations of a smaller target list of 40 key stars, including at least 10 M dwarfs, to characterize flares and variability on day timescales.
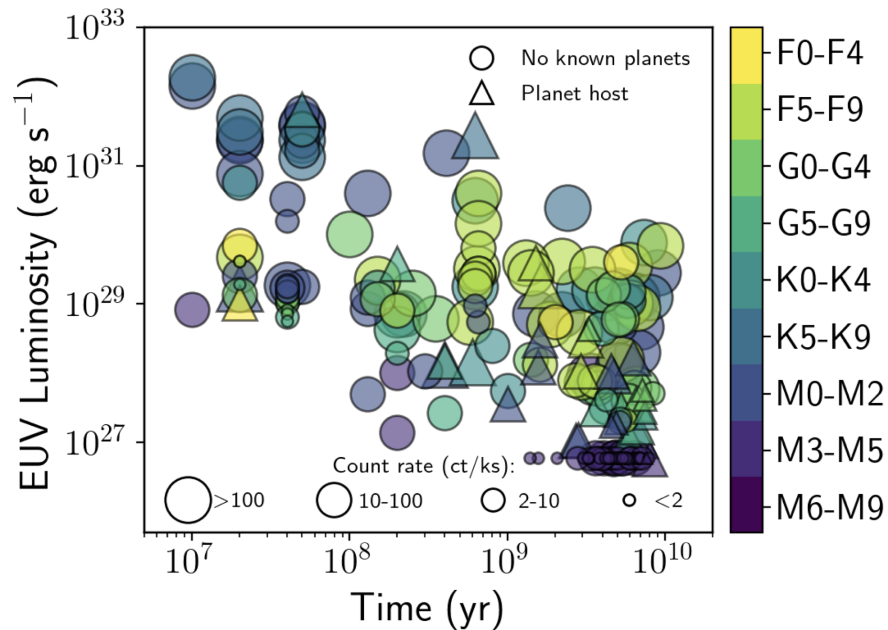
Fig 14 The estimated EUV luminosities and NExtUP Channel B count rates of a provisional sample of 200 potential NExtUP F-M-type target stars as a function of stellar age, demonstrating the capability of NExtUP to map out EUV emission over the relevant stellar parameter space.

NExUS   will acquire sufficient signal to measure fluxes for ultracool low-mass M dwarfs (M6 V and later) whose faintness requires longer observations than typical for SHINE targets.

NExtOP   will perform EUV observations in concert with other facilities, such as JWST during exoplanet transit campaigns, or for short notice targets of opportunity.

Target selection for NExtUP would be dictated by: (1) observability of a star of interest in the EUV through the intervening ISM; (2) importance as an exoplanet host star; and (3) importance for mapping out EUV behavior and characteristics as a function of spectral type and magnetic activity level. Estimated EUV luminosities and predicted NExtUP Channel B count rates for a provisional sample of 200 nearby F-M-type stars are illustrated in Figure 14.

Full target lists would be a subject of Phase A study, taking advantage of emerging and future advances in planet detection and characterization. A list of 200 provisional SHINE targets covering spectral types F to mid-M, including a number of prominent exoplanet hosts, together with a list of 20 potential late-M NExUS targets and 40 LONESTAR candidates.

Exposures would be based on achieving S/N=10 in Channel B (226-302Å) which ensures at least Channels A (less susceptible to ISM absorption) and 304 Å are observable, the latter generally yielding similar S/N and counts as Channel B. S/N=10 ensures reconstruction of fluxes across the EUV band is accurate to a similar precision.

NExtUP is ready to be proposed as a smallsat, either through a dedicated AO, or as a Mission of Opportunity. With a relatively short required development time, NExtUP could overlap with the nominal JWST mission, at the time of writing slated to run from late 2021 to late 2026 (but with likely extension).

7 Secondary Science Opportunities

7.1 Coronal Dimming and Flares

NExtUP is expected to observe many flares on stars, especially during long stare observations, and should be able to detect coronal dimming due to coronal mass ejections (CMEs) in the case of very large events. CMEs are very difficult to detect on stars but could be quite critical for exoplanet space weather, especially on planets around M dwarf stars with close-in habitable zones. Theoretical studies have indicated that CMEs on magnetically active stars might be suppressed [75, 76, 77], making detections of CMEs crucial for understanding their true impact on planets. Coronal dimming has recently been tentatively detected in several stellar events based on archival data, with dimming amounting to more than

10% of the quiescent flux [78]. Through coronal dimming, NExtUP would provide a new window into exoplanet space weather.

7.2 ISM, B stars and Hot White Dwarfs

NExtUP will provide estimates of the absorption in the ISM in the line of sight to stars it will observe. This would constitute by far the most extensive set of ISM absorption measurements in the solar vicinity. Hot white dwarfs can also provide key ISM absorption information, with the ensemble data providing a detailed map of the structure of the local interstellar gas in which the Sun presently resides.

The local ISM is ionized and sculpted by the EUV flux from hot stars, including white dwarfs and B stars [79, 80]. NExtUP will be able to perform a sensitive survey of white dwarf and B star EUV emission down to limits two or more orders of magnitude than reached by EUVE that can provide key information for understanding the local ISM ionization. The stellar EUV radiation field (80–912 Å) at the Earth measured by EUVE found that, for wavelengths > 500 Å it is dominated by contributions from two early type-B stars (ϵ and β CMa), and for wavelengths < 500 Å, local hot white dwarfs are the major contributor [79, 80].

NExtUP will also enable the study of white dwarf atmospheres in a waveband not observed for two decades. This region of their spectra can be dominated by metals levitated against gravity by the radiation field [e.g., 81] and NExtUP photometry can provide powerful constraints for diffusion and model atmosphere theory.

7.3 Solar System Science

NExtUP would be the first EUV astrophysics observatory since EUVE was deactivated on 2001 January 31, and will have the highest spatial resolution of any such facility to date (8" vs $\sim$ 30-60" for EUVE).

With 8" imaging, NExtUP can spatially resolve EUV emission on other compelling targets that are also of high relevance to NExtUP science goals of understanding planetary atmospheric loss. NExtUP is capable of resolving EUV emission on Venus, Mars and Jupiter (O II 834 Å, He II 304 Å and in principle He I 584 Å, although NExtUP is designed to suppress this emission), the Io Torus (several ions including S III 678 Å and O II 834 Å), and from comets (He and other ions). Exposures to reach S/N=10 per resolution element range from minutes to $\sim$100ks.

7.3.1 Venus

From Earth orbit, NExtUP observations of Venus would likely be made near elongation, when Venus is half sunlit and about 25" in diameter (the Venus airglow layer peaks at an altitude of $\sim$ 100 km [82], which would provide $\sim$ 7 resolution elements over the entire disk. Venus has only been occasionally observed at EUV wavelengths, most notably with the Hopkins Ultraviolet Telescope (HUT) during the Astro-2 shuttle mission [83] over the 820–1840 Å spectral range; during the 1999 Cassini flyby [84] using the UV Imaging Spectrograph (UVIS) over the 800-1300 Å spectral range; at shorter wavelengths with the Extreme Ultraviolet Explorer (EUVE) observatory [85]; and, more recently using the Extreme Ultraviolet Spectroscope for Exospheric Dynamics (EXCEED) spectrograph on the Hisaki observatory [86].

Based on the NExtUP sensitivity, a useful scientific study of Venus would be several observations at both elongations to map the distribution in local time of EUV emission, which is expected to exhibit a bulge at a few hours past midnight, due to dynamics. In addition, the observations would test the EUVE observations of 304 Å helium ion emission, which were surprisingly bright [82].

7.3.2 The Moon

Surprisingly, the Moon has been observed only very infrequently at EUV wavelengths (LRO-LAMP has MgF2-coated optics, so is very insensitive at wavelengths < 1150 Å, although it is able to detect the He 584 Å lunar exosphere emission). The Moon was imaged with EUVE and found to have an albedo pattern reversed from that at visible wavelengths [i.e., at EUV wavelengths, mare are more reflective than highlands; 88]. Similar results were obtained for the shortest EUV wavelengths around $\sim$ 100 Å using the *Chandra* HRC-I (Figure 15).

Observing the Moon with NExtUP would greatly improve on the EUVE data with much higher spatial resolution and greater phase angle coverage and much more extensive exposure times and longer wavelength coverage than afforded by *Chandra*. Note that the Moon would approximately fill the NExtUP field of view, so rastered or scanned observations would be needed.
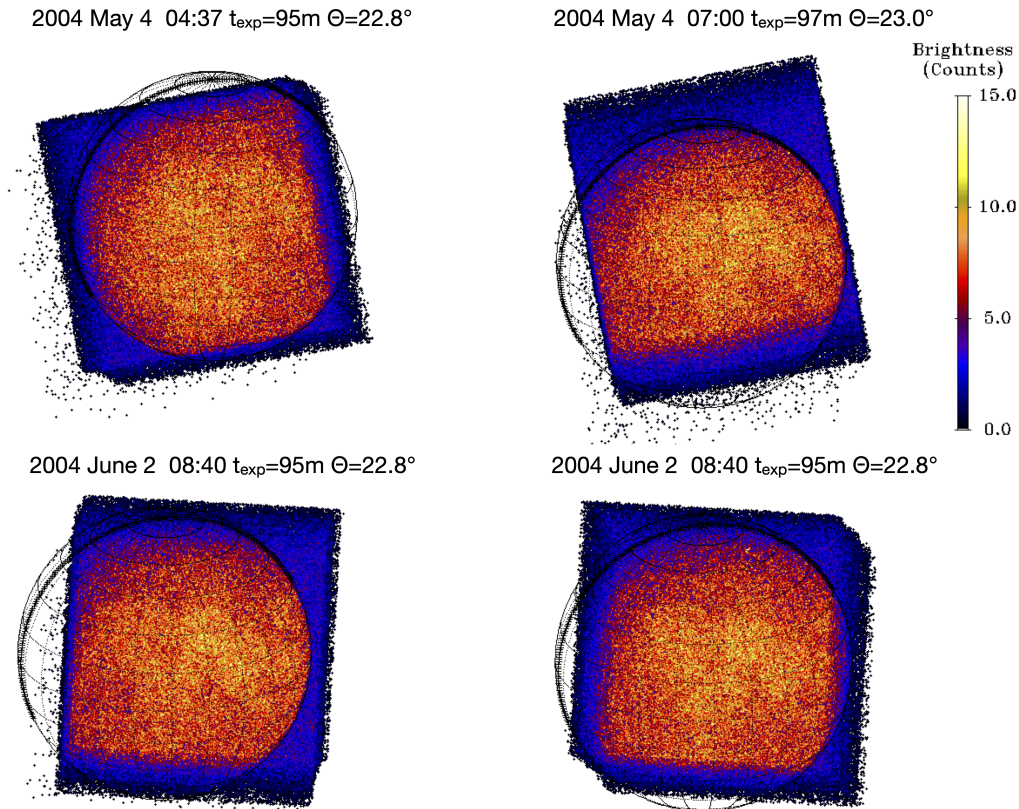
Fig 15 Chandra images of the Moon with the *Chandra* HRC-I at an effective wavelength of ~ 100 Å demonstrating the albedo reversal between mare and highlands compared with visible light [87].

7.3.3 Mars

From Earth orbit, NExtUP observations of Mars would likely be made near opposition, when Mars is fully sunlit and about 18" in diameter (the Martian airglow layer peaks at an altitude of ~ 100 km [82], which would marginally resolve the planet with ~ 4 resolution elements over the disk. As for Venus, Mars has only been occasionally observed at EUV wavelengths, with the Hopkins Ultraviolet Telescope (HUT) during the Astro-2 shuttle mission [83] over the 820–1840 Å spectral range; with the Far Ultraviolet Spectrographic Explorer (FUSE) observatory at very high resolution over the 900–1200 Å spectral range [89]; and at shorter wavelengths with EUVE [85].

Based on the NExtUP sensitivity, a useful scientific study of Mars would be several observations at opposition to study the 304 Å helium emission and O II 834 Å emission, which might provide clues from which the escape rates of helium and oxygen can be estimated, and compared with earlier EUVE results [85] and with the escape rate of hydrogen determined from MAVEN in-situ observations.

7.3.4 Jupiter and the Io Torus

Near opposition, the diameter of Jupiter as seen from Earth is about 47" so NExtUP images would cover the disk with ~ 27 pixels 8" in size. The helium emission at 58.4 nm at Jupiter has been observed by EUVE, but at rather poorer spatial resolution [90], but will likely be very faint due to the designed suppression in NExtUP. O II 834 Å should instead be detectable. Such features are particularly useful at Jupiter, as their brightness is a straightforward proxy for the strength of turbulence (or eddy diffusion) in the upper atmosphere (i.e., overlying atomic and molecular hydrogen absorb such photons, so anywhere the emitting gas is mixed upward from below will reflect more of the solar flux. Cassini observations [91] and recent Juno observations [92] suggest the eddy diffusion may be particularly large in the auroral regions, and NExtUP observations could test this. Further, it seems plausible that Jovian He II 304 Å emission may be detectable with NExtUP, as these would also be expected in the auroral regions.

7.3.5 Io Plasma Torus

The Io Plasma Torus (IPT) has been observed at EUV wavelengths (where it is brightest) by EUVE [93], but was perhaps best observed during the Cassini flyby [94] and more recently with Hisaki-EXCEED [95]. At opposition, the entire IPT is about 50"×300", and would comfortably fit in the NExtUP field of view. Currently, most IPT research involves synoptic studies (e.g., several years of daily monitoring by Hisaki), which might be difficult for NExtUP. However, if there were a volcanic outburst during the NExtUP mission, the IPT response would make an excellent target of opportunity.

8 Summary

NASA SmallSat initiatives provide an opportunity for important focused science experiments within a low cost envelope. NExtUP addresses a critical area of exoplanet science: the energetic EUV photon environment that drives atmospheric loss. NExtUP combines very simple prime focus optics with cutting-edge multilayer coatings to produce an EUV telescope orders of magnitude more sensitive than EUVE that can map out EUV emission in stars over the full range of F-M spectral types and ages. NExtUP could also undertake a compelling array of secondary science.

References

[1] A. Segura, J. F. Kasting, V. Meadows, *et al.*, "Biosignatures from Earth-Like Planets Around M Dwarfs," *Astrobiology* **5**, 706–725 (2005).

[2] R. Hu, S. Seager, and W. Bains, "Photochemistry in Terrestrial Exoplanet Atmospheres. I. Photochemistry Model and Benchmark Cases," ApJ **761**, 166 (2012).

[3] F. Tian, K. France, J. L. Linsky, *et al.*, "High stellar FUV/NUV ratio and oxygen contents in the atmospheres of potentially habitable planets," *Earth and Planetary Science Letters* **385**, 22–27 (2014).

[4] C. E. Harman, E. W. Schwieterman, J. C. Schottelkotte, *et al.*, "Abiotic O$_2$ Levels on Planets around F, G, K, and M Stars: Possible False Positives for Life?," ApJ **812**, 137 (2015).

[5] V. S. Meadows, G. N. Arney, E. W. Schwieterman, *et al.*, "The Habitability of Proxima Centauri b: Environmental States and Observational Discriminants," *Astrobiology* **18**, 133–189 (2018).

[6] H. Lammer, J. H. Bredehöft, A. Coustenis, *et al.*, "What makes a planet habitable?," A&A Rev. **17**, 181–249 (2009).

[7] G. Gronoff, P. Arras, S. Baraka, *et al.*, "Atmospheric Escape Processes and Planetary Atmospheric Evolution," *Journal of Geophysical Research (Space Physics)* **125**, e27639 (2020).

[8] A. Vidal-Madjar, J. M. Désert, A. Lecavelier des Etangs, *et al.*, "Detection of Oxygen and Carbon in the Hydrodynamically Escaping Atmosphere of the Extrasolar Planet HD 209458b," ApJ **604**, L69–L72 (2004).

[9] J. L. Linsky, H. Yang, K. France, *et al.*, "Observations of Mass Loss from the Transiting Exoplanet HD 209458b," ApJ **717**, 1291–1299 (2010).

[10] G. E. Ballester and L. Ben-Jaffel, "Re-visit of HST FUV Observations of the Hot-Jupiter System HD 209458: No Si III Detection and the Need for COS Transit Observations," ApJ **804**, 116 (2015).

[11] Y. N. Kulikov, H. Lammer, H. I. M. Lichtenegger, *et al.*, "Atmospheric and water loss from early Venus," Planet. Space Sci. **54**, 1425–1444 (2006).

[12] C. Dong, M. Lingam, Y. Ma, *et al.*, "Is Proxima Centauri b Habitable? A Study of Atmospheric Loss," ApJ **837**, L26 (2017).

[13] T. N. Woods, P. C. Chamberlin, J. W. Harder, *et al.*, "Solar Irradiance Reference Spectra (SIRS) for the 2008 Whole Heliosphere Interval (WHI)," Geophys. Res. Lett. **36**, L01101 (2009).

[14] J. M. Fontenla, J. L. Linsky, J. Witbrod, *et al.*, "Semi-empirical Modeling of the Photosphere, Chromosphere, Transition Region, and Corona of the M-dwarf Host Star GJ 832," ApJ **830**, 154 (2016).

[15] C. P. Johnstone, M. Güdel, A. Stökl, *et al.*, "The Evolution of Stellar Rotation and the Hydrogen Atmospheres of Habitable-zone Terrestrial Planets," ApJ **815**, L12 (2015).

[16] B. M. Jakosky, D. Brain, M. Chaffin, *et al.*, "Loss of the Martian atmosphere to space: Present-day loss rates determined from MAVEN observations and integrated loss through time," Icarus **315**, 146–157 (2018).

[17] L. Tu, C. P. Johnstone, M. Güdel, *et al.*, "The extreme ultraviolet and X-ray Sun in Time: High-energy evolutionary tracks of a solar-like star," A&A **577**, L3 (2015).

[18] U. V. Amerstorfer, H. Gröller, H. Lichtenegger, *et al.*, "Escape and evolution of Mars's CO_2 atmosphere: Influence of suprathermal atoms," *Journal of Geophysical Research (Planets)* **122**, 1321–1337 (2017).

[19] D. Deming, S. Seager, J. Winn, *et al.*, "Discovery and Characterization of Transiting Super Earths Using an All-Sky Transit Survey and Follow-up by the James Webb Space Telescope," PASP **121**, 952 (2009).

[20] A. R. Belu, F. Selsis, J. C. Morales, *et al.*, "Primary and secondary eclipse spectroscopy with JWST: exploring the exoplanet parameter space," A&A **525**, A83 (2011).

[21] I. Snellen, R. de Kok, J. L. Birkby, *et al.*, "Combining high-dispersion spectroscopy with high contrast imaging: Probing rocky planets around our nearest neighbors," A&A **576**, A59 (2015).

[22] K. France, N. Arulanantham, L. Fossati, *et al.*, "Far-ultraviolet Activity Levels of F, G, K, and M Dwarf Exoplanet Host Stars," ApJS **239**, 16 (2018).

[23] V. S. Airapetian, A. Glocer, G. V. Khazanov, *et al.*, "How Hospitable Are Space Weather Affected Habitable Zones? The Role of Ion Escape," ApJ **836**, L3 (2017).

[24] K. Garcia-Sage, A. Glocer, J. J. Drake, *et al.*, "On the Magnetic Protection of the Atmosphere of Proxima Centauri b," ApJ **844**, L13 (2017).

[25] J. J. Drake, V. L. Kashyap, B. J. Wargelin, *et al.*, "Pointing Chandra toward the Extreme Ultraviolet Fluxes of Very Low Mass Stars," ApJ **893**, 137 (2020).

[26] J. L. Linsky, J. Fontenla, and K. France, "The Intrinsic Extreme Ultraviolet Fluxes of F5 V TO M5 V Stars," ApJ **780**, 61 (2014).

[27] J. Sanz-Forcada, G. Micela, I. Ribas, *et al.*, "Estimation of the XUV radiation onto close planets and their evaporation," A&A **532**, A6 (2011).

[28] I. Ribas, M. D. Gregg, T. S. Boyajian, *et al.*, "The full spectral radiative properties of Proxima Centauri," A&A **603**, A58 (2017).

[29] R. M. Ramirez and L. Kaltenegger, "The Habitable Zones of Pre-main-sequence Stars," ApJ **797**, L25 (2014).

[30] R. Luger and R. Barnes, "Extreme Water Loss and Abiotic O2Buildup on Planets Throughout the Habitable Zones of M Dwarfs," *Astrobiology* **15**, 119–143 (2015).

[31] R. D. Wordsworth, L. K. Schaefer, and R. A. Fischer, "Redox Evolution via Gravitational Differentiation on Low-mass Planets: Implications for Abiotic Oxygen, Water Loss, and Habitability," AJ **155**, 195 (2018).

[32] S. Bowyer and R. F. Malina, "The extreme ultraviolet explorer mission," *Advances in Space Research* **11**, 205–215 (1991).

[33] S. Bowyer, J. J. Drake, and S. Vennes, "Extreme Ultraviolet Astronomy," ARA&A **38**, 231–288 (2000).

[34] J. J. Drake, J. M. Laming, and K. G. Widing, "Stellar Coronal Abundances. II. The First Ionization Potential Effect and Its Absence in the Corona of Procyon," ApJ **443**, 393 (1995).

[35] J. J. Drake, J. M. Laming, and K. G. Widing, "Stellar Coronal Abundances. V. Evidence for the First Ionization Potential Effect in α Centauri," ApJ **478**, 403–416 (1997).

[36] L. M. Walkowicz and S. L. Hawley, "Tracers of Chromospheric Structure. I. Observations of Ca II K and Hα in M Dwarfs," AJ **137**, 3297–3313 (2009).

[37] K. France, R. O. P. Loyd, A. Youngblood, *et al.*, "The MUSCLES Treasury Survey. I. Motivation and Overview," ApJ **820**, 89 (2016).

[38] S. Peacock, T. Barman, E. L. Shkolnik, *et al.*, "Predicting the Extreme Ultraviolet Radiation Environment of Exoplanets around Low-mass Stars: The TRAPPIST-1 System," ApJ **871**, 235 (2019).

[39] G. W. King, P. J. Wheatley, M. Salz, *et al.*, "The XUV environments of exoplanets from Jupiter-size to super-Earth," MNRAS **478**, 1193–1208 (2018).

[40] B. E. Wood, S. Redfield, J. L. Linsky, *et al.*, "Stellar Lyα Emission Lines in the Hubble Space Telescope Archive: Intrinsic Line Fluxes and Absorption from the Heliosphere and Astrospheres," ApJS **159**, 118–140 (2005).

[41] J. L. Linsky, S. Redfield, and D. Tilipman, "The Interface between the Outer Heliosphere and the Inner Local ISM: Morphology of the Local Interstellar Cloud, Its Hydrogen Hole, Strömgren Shells, and ^{60}Fe Accretion," ApJ **886**, 41 (2019).

[42] F. C. Bruhweiler and K.-P. Cheng, "The Stellar Radiation Field and the Ionization of H and He in the Local Interstellar Medium," ApJ **335**, 188 (1988).

[43] S. Redfield and J. L. Linsky, "The Three-dimensional Structure of the Warm Local Interstellar Medium. II. The Colorado Model of the Local Interstellar Cloud," ApJ **534**, 825–837 (2000).

[44] S. Redfield and J. L. Linsky, "The Structure of the Local Interstellar Medium. IV. Dynamics, Morphology, Physical Properties, and Implications of Cloud-Cloud Interactions," ApJ **673**, 283–314 (2008).

[45] B. Y. Welsh, R. Lallement, J. L. Vergely, *et al.*, "New 3D gas density maps of NaI and CaII interstellar absorption within 300 pc," A&A **510**, A54 (2010).

[46] K. Kobayashi, J. Cirtain, A. R. Winebarger, *et al.*, "The High-Resolution Coronal Imager (Hi-C)," Sol. Phys. **289**, 4393–4412 (2014).

[47] R. Soufli, M. Fernández-Perea, S. L. Baker, *et al.*, "Spontaneously intermixed Al-Mg barriers enable corrosion-resistant Mg/SiC multilayer coatings," *Applied Physics Letters* **101**, 043111 (2012).

[48] K. Le Guen, M. H. Hu, J. M. André, *et al.*, "Introduction of Zr in nanometric periodic Mg/Co multilayers," *Applied Physics A: Materials Science & Processing* **102**, 69–77 (2011).

[49] N. Erickson, J. Green, K. France, *et al.*, "The Dual-channel Extreme Ultraviolet Continuum Experiment: Sounding rocket EUV observations of local B stars to determine their potential for supplying intergalactic ionizing radiation," in *UV, X-Ray, and Gamma-Ray Space Instrumentation for Astronomy XXI*, *Society of Photo-Optical Instrumentation Engineers (SPIE) Conference Series* **11118**, 111180S (2019).

[50] B. T. Fleming, K. France, N. Nell, *et al.*, "SISTINE: a pathfinder for FUV imaging spectroscopy on future NASA astrophysics missions," in *Space Telescopes and Instrumentation 2016: Ultraviolet to Gamma Ray*, J.-W. A. den Herder, T. Takahashi, and M. Bautz, Eds., *Society of Photo-Optical Instrumentation Engineers (SPIE) Conference Series* **9905**, 99050A (2016).

[51] J. V. Vallerga, J. B. McPhate, A. P. Martin, *et al.*, "HST-COS far-ultraviolet detector: final ground calibration," in *UV/EUV and Visible Space Instrumentation for Astronomy and Solar Physics*, O. H. Siegmund, S. Fineschi, and M. A. Gummin, Eds., *Society of Photo-Optical Instrumentation Engineers (SPIE) Conference Series* **4498**, 141–151 (2001).

[52] O. H. Siegmund, P. N. Jelinsky, S. R. Jelinsky, *et al.*, "High-resolution cross delay line detectors for the GALEX mission," in *EUV, X-Ray, and Gamma-Ray Instrumentation for Astronomy X*, O. H. Siegmund and K. A. Flanagan, Eds., *Society of Photo-Optical Instrumentation Engineers (SPIE) Conference Series* **3765**, 429–440 (1999).

[53] P. N. Jelinsky, P. F. Morrissey, J. M. Malloy, *et al.*, "Performance results of the GALEX cross delay line detectors," in *Future EUV/UV and Visible Space Astrophysics Missions and Instrumentation.*, J. C. Blades and O. H. W. Siegmund, Eds., *Society of Photo-Optical Instrumentation Engineers (SPIE) Conference Series* **4854**, 233–240 (2003).

[54] O. H. W. Siegmund, B. Y. Welsh, C. Martin, *et al.*, "The GALEX mission and detectors," in *UV and Gamma-Ray Space Telescope Systems*, G. Hasinger and M. J. L. Turner, Eds., *Society of Photo-Optical Instrumentation Engineers (SPIE) Conference Series* **5488**, 13–24 (2004).

[55] O. H. W. Siegmund, J. McPhate, T. Curtis, *et al.*, "Ultraviolet imaging detectors for the GOLD mission," in *Space Telescopes and Instrumentation 2016: Ultraviolet to Gamma Ray*, J.-W. A. den Herder, T. Takahashi, and M. Bautz, Eds., *Society of Photo-Optical Instrumentation Engineers (SPIE) Conference Series* **9905**, 99050D (2016).

[56] N. T. Darling, O. H. W. Siegmund, T. Curtis, *et al.*, "Microchannel plate life testing for UV spectroscopy instruments," in *Society of Photo-Optical Instrumentation Engineers (SPIE) Conference Series*, *Society of Photo-Optical Instrumentation Engineers (SPIE) Conference Series* **10397**, 1039712 (2017).

[57] O. H. W. Siegmund, K. Coburn, and R. F. Malina, "Investigation of large format microchannel plate Z configurations," *IEEE Transactions on Nuclear Science* **32**, 443–447 (1985).

[58] M. E. Caldwell, N. Morris, D. K. Griffin, *et al.*, "The VUV instrument SPICE for Solar Orbiter: performance ground testing," in *Society of Photo-Optical Instrumentation Engineers (SPIE) Conference Series*, *Society of Photo-Optical Instrumentation Engineers (SPIE) Conference Series* **10397**, 1039708 (2017).

[59] R. A. Harrison, E. C. Sawyer, M. K. Carter, *et al.*, "The Coronal Diagnostic Spectrometer for the Solar and Heliospheric Observatory," Sol. Phys. **162**, 233–290 (1995).

[60] M. M. Sirk, E. J. Korpela, Y. Ishikawa, *et al.*, "Design and Performance of the ICON EUV Spectrograph," Space Sci. Rev. **212**, 631–643 (2017).

[61] C. D. Ertley, A. V. Lyashenko, B. W. Adams, *et al.*, "Developments in large-area flat panel photodetectors with ALD glass capillary array microchannel plates," in *UV, X-Ray, and Gamma-Ray Space Instrumentation for Astronomy XXI*, *Society of Photo-Optical Instrumentation Engineers (SPIE) Conference Series* **11118**, 111180L (2019).

[62] M. W. Davis, G. R. Gladstone, T. K. Greathouse, *et al.*, "Radiometric performance results of the Juno ultraviolet spectrograph (Juno-UVS)," in *Society of Photo-Optical Instrumentation Engineers (SPIE) Conference Series*, *Society of Photo-Optical Instrumentation Engineers (SPIE) Conference Series* **8146**, 814604 (2011).

[63] M. W. Davis, O. H. W. Siegmund, G. R. Gladstone, *et al.*, "Bench and thermal vacuum testing of the JUICE-UVS microchannel plate detector system," in *UV, X-Ray, and Gamma-Ray Space Instrumentation for Astronomy XXI*, *Society of Photo-Optical Instrumentation Engineers (SPIE) Conference Series* **11118**, 111180Q (2019).

[64] R. Gladstone, K. Retherford, J. Eterno, *et al.*, "The Ultraviolet Spectrograph on the JUICE Mission (JUICE-UVS)," in *European Planetary Science Congress*, EPSC2013–394 (2013).

[65] T. Bayer, M. Bittner, B. Buffington, *et al.*, "Europa Clipper Mission: Preliminary Design Report," in *2019 IEEE Aerospace Conference*, 1–24 (2019).

[66] K. D. Retherford, R. Gladstone, T. K. Greathouse, *et al.*, "The Ultraviolet Spectrograph on the Europa Mission (Europa-UVS)," in *AGU Fall Meeting Abstracts*, **2015**, P13E–02 (2015).

[67] S. A. Stern, D. C. Slater, J. Scherrer, *et al.*, "ALICE: The Ultraviolet Imaging Spectrograph Aboard the New Horizons Pluto-Kuiper Belt Mission," Space Sci. Rev. **140**, 155–187 (2008).

[68] G. R. Gladstone, S. A. Stern, K. D. Retherford, *et al.*, "LAMP: The Lyman Alpha Mapping Project on NASA's Lunar Reconnaissance Orbiter Mission," Space Sci. Rev. **150**, 161–181 (2010).

[69] O. H. W. Siegmund, E. Everman, J. V. Vallerga, *et al.*, "Ultraviolet quantum detection efficiency of potassium bromide as an opaque photocathode applied to microchannel plates," Appl. Opt. **26**, 3607–3614 (1987).

[70] S. R. Jelinsky, O. H. Siegmund, and J. A. Mir, "Progress in soft x-ray and UV photocathodes," in *EUV, X-Ray, and Gamma-Ray Instrumentation for Astronomy VII*, O. H. Siegmund and M. A. Gummin, Eds., *Society of Photo-Optical Instrumentation Engineers (SPIE) Conference Series* **2808**, 617–625 (1996).

[71] C. D. Ertley, O. H. W. Siegmund, S. R. Jelinsky, *et al.*, "Second generation large area microchannel plate flat panel phototubes," in *High Energy, Optical, and Infrared Detectors for Astronomy VII*, A. D. Holland and J. Beletic, Eds., *Society of Photo-Optical Instrumentation Engineers (SPIE) Conference Series* **9915**, 99152G (2016).

[72] B. T. Fleming, K. France, J. Williams, *et al.*, "High-sensitivity far-ultraviolet imaging spectroscopy with the SPRITE Cubesat," in *UV, X-Ray, and Gamma-Ray Space Instrumentation for Astronomy XXI*, *Society of Photo-Optical Instrumentation Engineers (SPIE) Conference Series* **11118**, 111180U (2019).

[73] J. Williams, B. T. Fleming, D. Vorobiev, *et al.*, "Design, implementation, and validation of the electronics for the SPRITE CubeSat," in *Society of Photo-Optical Instrumentation Engineers (SPIE) Conference Series*, *Society of Photo-Optical Instrumentation Engineers (SPIE) Conference Series* **11444**, 1144454 (2020).

[74] J. C. Green, N. J. Nell, N. Erickson, *et al.*, "In-flight performance of a 200mm x 200mm microchannel plate detector," in *UV, X-Ray, and Gamma-Ray Space Instrumentation for Astronomy XXI*, *Society of Photo-Optical Instrumentation Engineers (SPIE) Conference Series* **11118**, 111180O (2019).

[75] J. J. Drake, O. Cohen, C. Garraffo, *et al.*, "Stellar flares and the dark energy of CMEs," in *Solar and Stellar Flares and their Effects on Planets*, A. G. Kosovichev, S. L. Hawley, and P. Heinzel, Eds., **320**, 196–201 (2016).

[76] J. D. Alvarado-Gómez, J. J. Drake, O. Cohen, *et al.*, "Suppression of Coronal Mass Ejections in Active Stars by an Overlying Large-scale Magnetic Field: A Numerical Study," ApJ **862**, 93 (2018).

[77] J. D. Alvarado-Gómez, J. J. Drake, S. P. Moschou, *et al.*, "Coronal Response to Magnetically Suppressed CME Events in M-dwarf Stars," ApJ **884**, L13 (2019).

[78] A. M. Veronig, P. Odert, M. Leitzinger, *et al.*, "Indications of stellar coronal mass ejections through coronal dimmings," *Nature Astronomy* (2021).

[79] J. Vallerga, "The Stellar Extreme-Ultraviolet Radiation Field," ApJ **497**, 921–927 (1998).

[80] B. Y. Welsh, J. Wheatley, N. J. Dickinson, *et al.*, "Ionization within the Local Cavity by Hot White Dwarfs," PASP **125**, 644 (2013).

[81] N. J. Dickinson, M. A. Barstow, and I. Hubeny, "The distribution of metals in hot DA white dwarfs," MNRAS **421**, 3222–3228 (2012).

[82] J. C. Gérard, S. W. Bougher, M. A. López-Valverde, *et al.*, "Aeronomy of the Venus Upper Atmosphere," Space Sci. Rev. **212**, 1617–1683 (2017).

[83] P. D. Feldman, E. B. Burgh, S. T. Durrance, *et al.*, "Far-Ultraviolet Spectroscopy of Venus and Mars at 4 Å Resolution with the Hopkins Ultraviolet Telescope on Astro-2," ApJ **538**, 395–400 (2000).

[84] J. C. Gérard, B. Hubert, J. Gustin, *et al.*, "EUV spectroscopy of the Venus dayglow with UVIS on Cassini," Icarus **211**, 70–80 (2011).

[85] V. A. Krasnopolsky and G. R. Gladstone, "Helium on Mars and Venus: EUVE observations and modeling," Icarus **176**, 395–407 (2005).

[86] K. Masunaga, K. Seki, N. Terada, *et al.*, "Periodic variations of oxygen EUV dayglow in the upper atmosphere of Venus: Hisaki/EXCEED observations," *Journal of Geophysical Research (Planets)* **120**, 2037–2052 (2015).

[87] J. Drake, G. R. Gladstone, S. A. Stern, *et al.*, "The First High Resolution Soft X-ray Images of the Moon," in *AAS/Division for Planetary Sciences Meeting Abstracts #36*, *AAS/Division for Planetary Sciences Meeting Abstracts* **36**, 39.09 (2004).

[88] B. C. Flynn, J. V. Vallerga, G. R. Gladstone, *et al.*, "Lunar reflectivity from Extreme Ultraviolet Explorer imaging and spectroscopy of the full moon," Geophys. Res. Lett. **25**, 3253–3256 (1998).

[89] V. A. Krasnopolsky and P. D. Feldman, "Far Ultraviolet Spectrum of Mars," Icarus **160**, 86–94 (2002).

[90] G. R. Gladstone, D. T. Hall, and J. Waite, J. Hunter, "EUVE Observations of Jupiter During the Impact of Comet Shoemaker-Levy 9," *Science* **268**, 1595–1597 (1995).

[91] C. D. Parkinson, A. I. F. Stewart, A. S. Wong, *et al.*, "Enhanced transport in the polar mesosphere of Jupiter: Evidence from Cassini UVIS helium 584 Å airglow," *Journal of Geophysical Research (Planets)* **111**, E02002 (2006).

[92] G. Clark, C. Tao, B. H. Mauk, *et al.*, "Precipitating Electron Energy Flux and Characteristic Energies in Jupiter's Main Auroral Region as Measured by Juno/JEDI," *Journal of Geophysical Research (Space Physics)* **123**, 7554–7567 (2018).

[93] F. Herbert, G. R. Gladstone, and G. E. Ballester, "Extreme Ultraviolet Explorer spectra of the Io plasma torus: Improved spectral resolution and new results," J. Geophys. Res. **106**, 26293–26309 (2001).

[94] A. J. Steffl, A. I. F. Stewart, and F. Bagenal, "Cassini UVIS observations of the Io plasma torus. I. Initial results," Icarus **172**, 78–90 (2004).

[95] I. Yoshikawa, F. Suzuki, R. Hikida, *et al.*, "Volcanic activity on Io and its influence on the dynamics of the Jovian magnetosphere observed by EXCEED/Hisaki in 2015," *Earth, Planets, and Space* **69**, 110 (2017).